Cell Reports, Volume *42*

Supplemental information

AXL-initiated paracrine activation of pSTAT3 enhances mesenchymal and vasculogenic supportive features of tumor-associated macrophages

Chia-Nung Hung, Meizhen Chen, Daniel T. DeArmond, Cheryl H.-L. Chiu, Catherine A. Limboy, Xi Tan, Meena Kusi, Chih-Wei Chou, Li-Ling Lin, Zhao Zhang, Chiou-Miin Wang, Chun-Liang Chen, Kohzoh Mitsuya, Pawel A. Osmulski, Maria E. Gaczynska, Nameer B. Kirma, Ratna K. Vadlamudi, Don L. Gibbons, Steve Warner, Andrew J. Brenner, Daruka Mahadevan, Joel E. Michalek, Tim H.-M. Huang, and Josephine A. Taverna

Figure S1 (related to Figure 1)

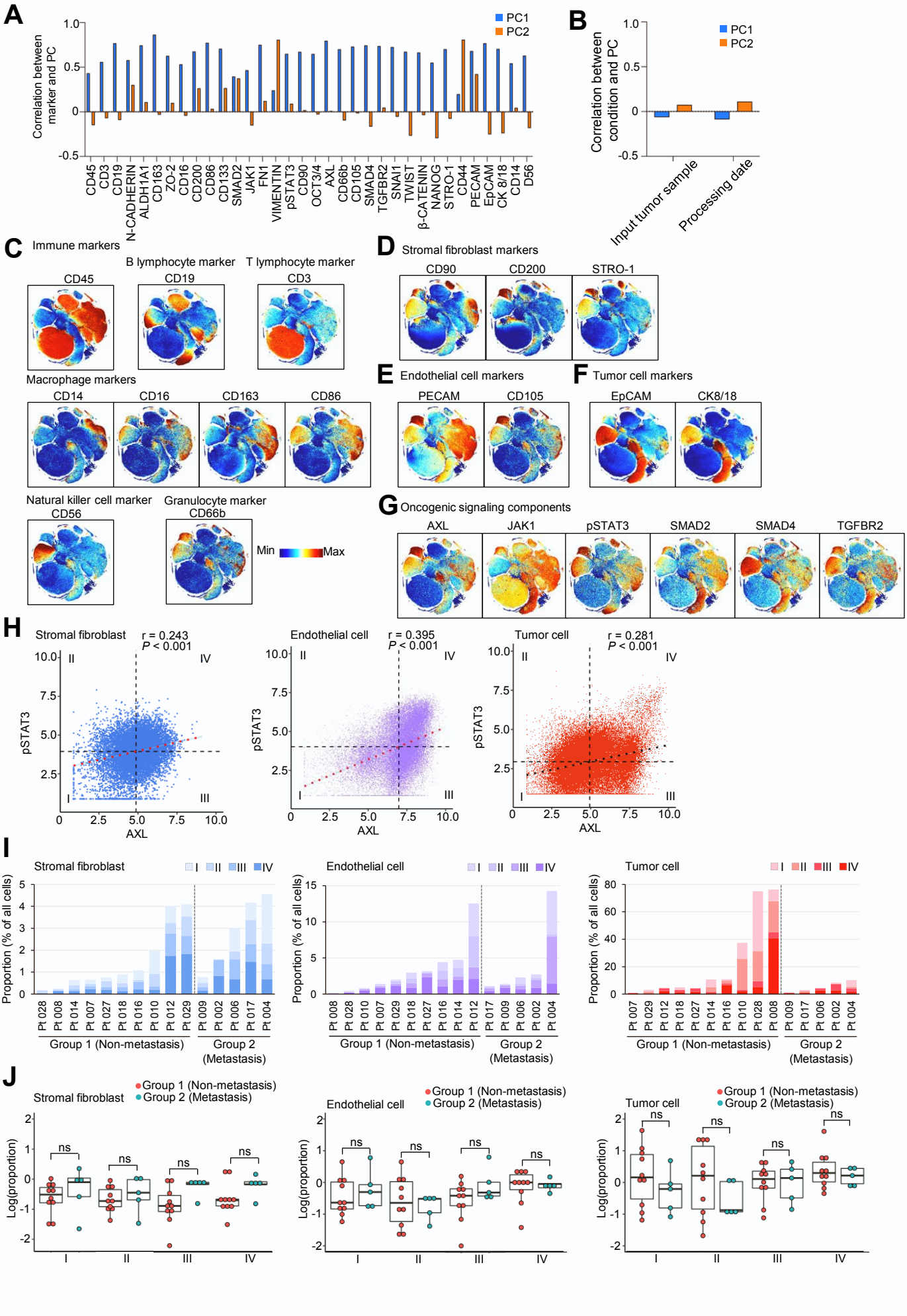

Figure S1. Cytometry by time-of-flight (CyTOF) single cell expression profiles of 34 protein markers of the 15 treatment-naïve lung tumors (related to Fig. 1).

(A) Bar graph of Spearman's correlation coefficients indicating all protein measurements from multiple CyTOF runs were highly correlated with the first two principal components (PCs) which in total explained 51% of the variance.

(B) Bar graph of Spearman's correlation coefficients between input tumor samples/processing dates and the first two PCs. Low correlations indicate minimal batch effect.

(C-F) t-distributed stochastic neighbor embedding (t-SNE) scatter plots of expression levels of surface markers for immune cells, stromal fibroblasts, and endothelial cells.

(G) t-SNE scatter plots of expression levels of oncogenic signaling markers.

(H) AXL and pSTAT3 correlation scatter plot of stromal fibroblasts, endothelial cells and tumor cells showing the four categories based on mean value of AXL and pSTAT3. $P < 0.001$.

(I) Bar graph of AXL-pSTAT3 category proportion of stromal fibroblasts, endothelial cells and tumor cells in individual patient. Group 1 and 2 tumors were classified based on TNM classification of individual patients. Group 1 tumors was non-metastatic patients and Group 2 tumors was patients with lymph node and/or distant metastasis. See also Supplementary Table S1.

(J) Box plot of category proportion of stromal fibroblasts, endothelial cells, and tumor cells between Group1 (n=10) and Group2 (n=5) tumors. Data are mean ± SD; Student's t test for each category.

Figure S2 (related to Figure 2)

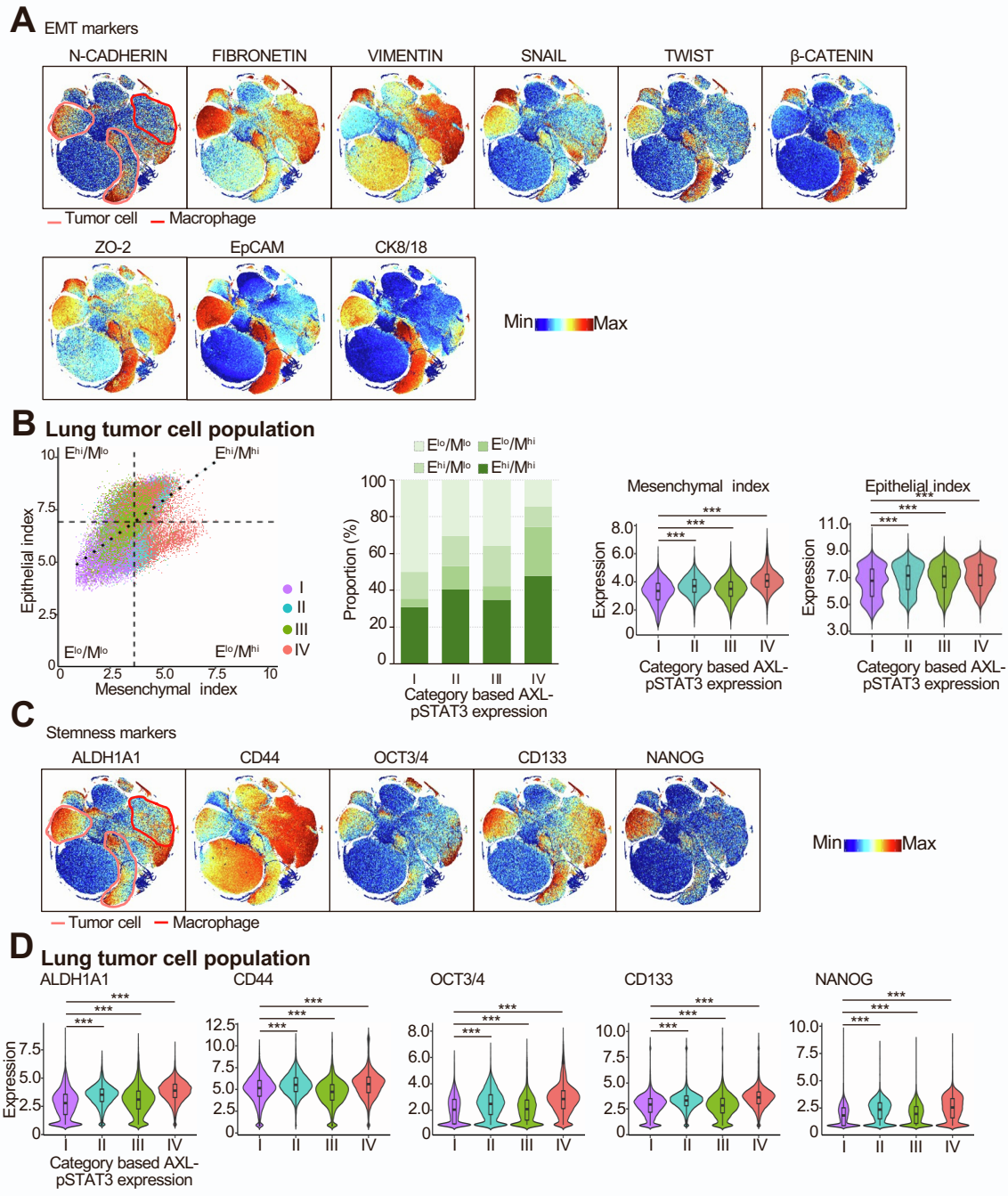

Figure S2. Concordant AXL and STAT3 was associated with intermediate epithelial-mesenchymal transition (EMT) and stemness features in tumor cells from the 15 lung tumors (related to Fig. 2).

(A) t-distributed stochastic neighbor embedding (t-SNE) scatter plots of expression levels of EMT markers.

(B) Mesenchymal index and epithelial index correlation scatter plot of tumor cells showing the four subtyoes based on mean value of mesenchymal index and epithelial index. $P < 0.001$. Bar graph of subtype proportion in four AXL-pSTAT3 categories. Violin plots of expression level of mesenchymal index and epithelial index in four AXL-pSTAT3 categories. Data are mean ± SD; ***$P < 0.001$; one-way ANOVA followed by Duncan's multiple range tests.

(C) t-SNE scatter plots of expression levels of stemness markers.

(D) Violin plots of expression level of stemness markers in four AXL-pSTAT3 categories. Data are mean ± SD; ***$P < 0.001$; one-way ANOVA followed by Duncan's multiple range tests.

Figure S3 (related to Figure 3)

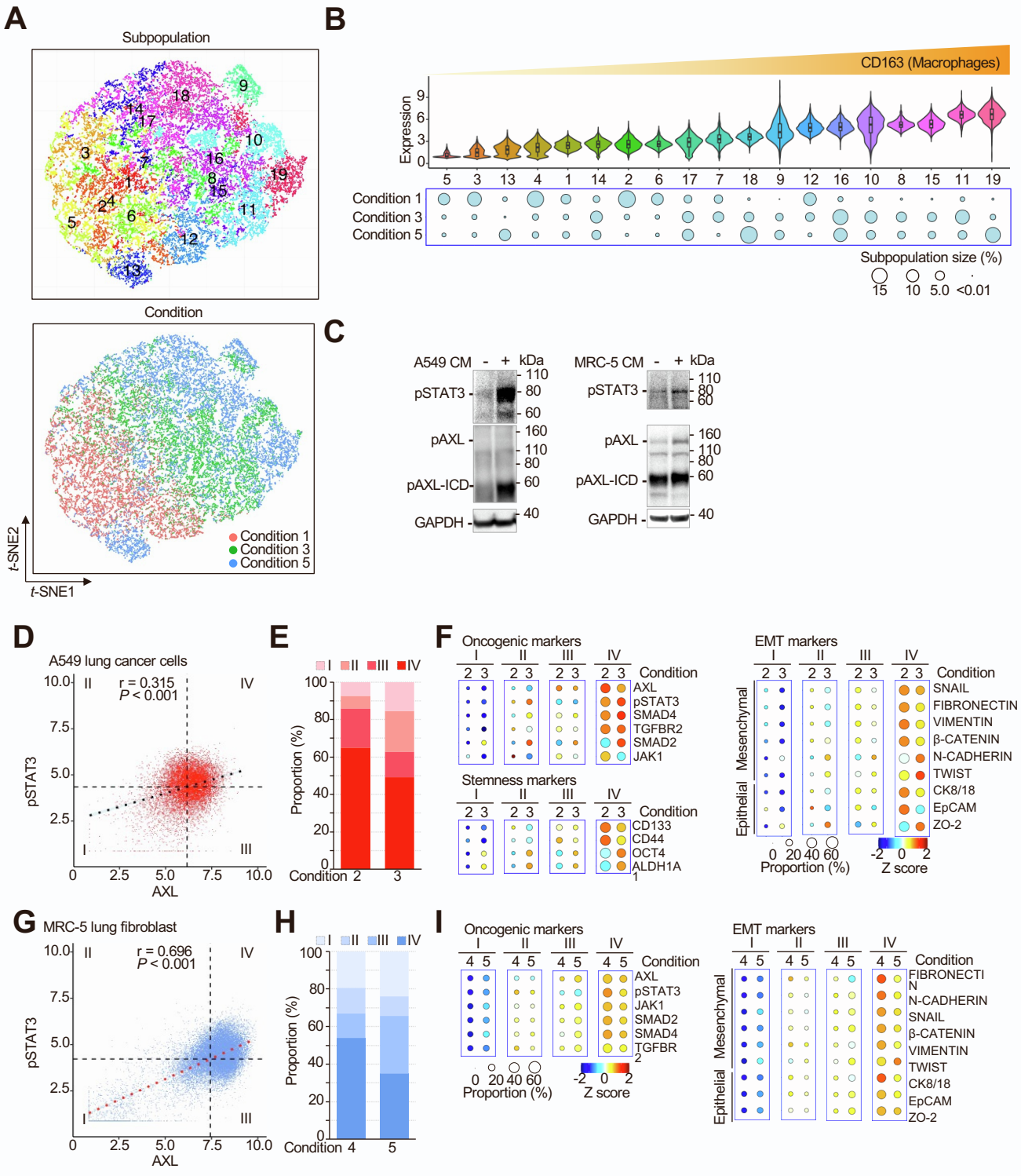

Figure S3. M0 macrophages exerted reciprocal influences on co-cultured A549 cells and MRC-5 fibroblasts (related to Fig. 3).

(A) t-distributed stochastic neighbor embedding (t-SNE) scatter plots of 19 subpopulations identified by PhenoGraph clustering algorithm in U937-derived macrophages of condition 1, 3 and 5.

(B) The 19 subpopulations of U937-derived macrophages of the 3 conditions were stratified based on increasing CD163 levels (violin plot).

(C) Western blots of phosphorylated AXL and STAT3 in U937-derived macrophages exposed to the conditioned medium of A549 lung cancer cells and MRC-5 lung fibroblasts.

(D) AXL and pSTAT3 correlation scatter plot of A549 lung cancer cells showing the four categories based on mean value of AXL and STAT3. $P < 0.001$.

(E) Bar graph of category proportion in condition 2 and 3.

(F) Circle plots showing the proportion and expression level of oncogenic, stemness and EMT markers of four AXL-pSTAT3 categories in A549 lung cancer cells from condition 2 and 3.

(G) AXL and pSTAT3 correlation scatter plot of MRC-5 lung fibroblasts showing the four categories based on mean value of AXL and STAT3. $P < 0.001$.

(H) Bar graph of category proportion in condition 4 and 5.

(I) Circle plots showing the proportion and expression level of oncogenic and EMT markers of four AXL-pSTAT3 categories in MRC-5 lung fibroblasts from condition 4 and 5.

Figure S4 (related to Figure 4)

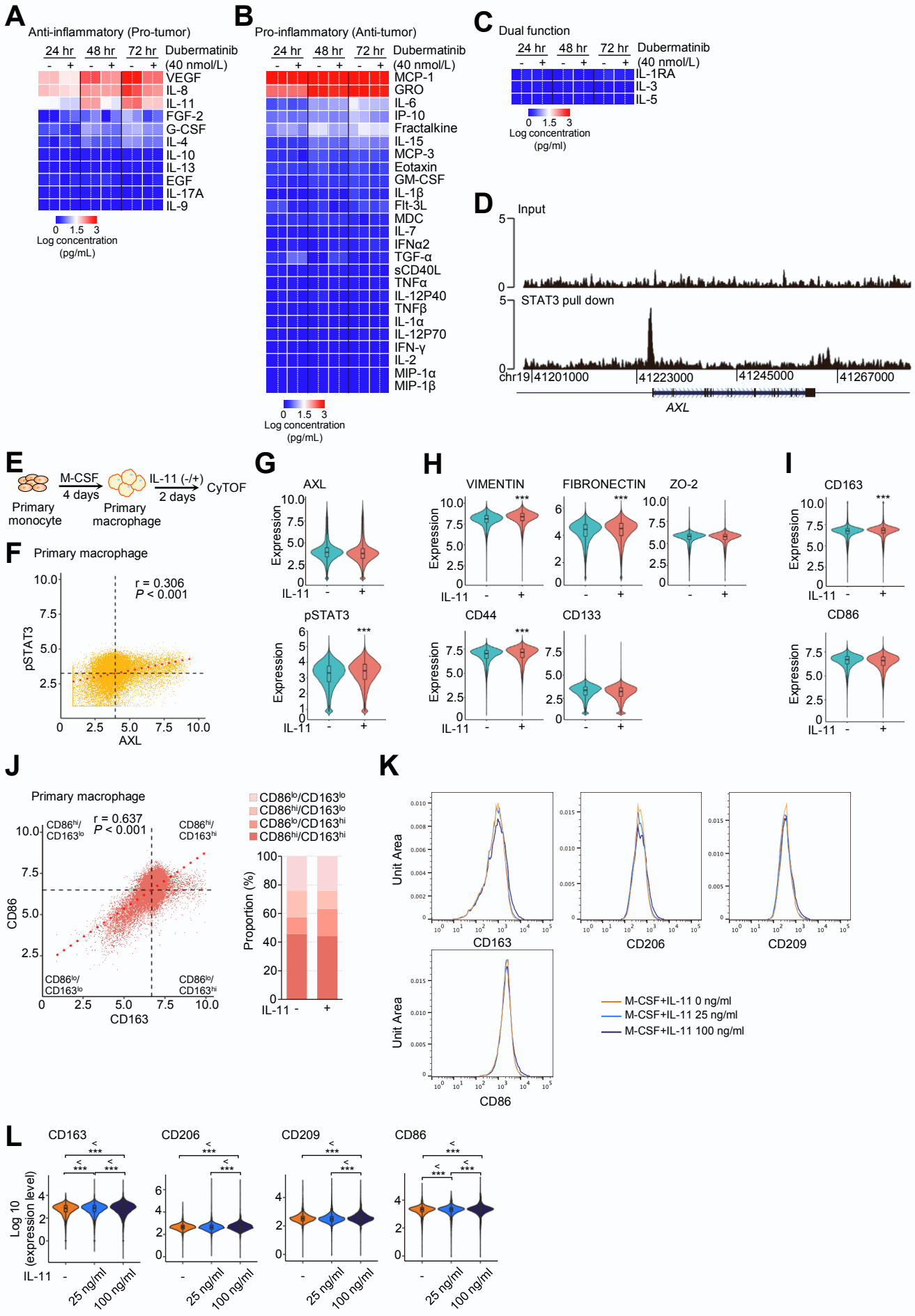

Figure S4. IL-11 elevate the expression level of macrophage plasticity markers in primary macrophages (related to Fig. 4).

(A-C) Expression heat maps of soluble factors and cytokines secreted from A549 lung cancer cells untreated and treated with AXL inhibitor, dubermatinib (40 nmol/L) for 24, 48 and 72 hr. IL-11 secretion by A549 cells was inhibited by dubermatinib.

(D) *In silico* analysis of anti-STAT3 ChIP-seq data indicates that anti-STAT3 immunoprecipitation enriched the promoter of *AXL*.

(E) Flow chart of primary macrophages induction and IL-11 treatment for CyTOF analysis.

(F) AXL and STAT3 correlation scatter plot of primary macrophages.

(G) Violin plots showing the expression level of AXL and STAT3 with and without IL-11 (25 ng/mL) exposure. Data are mean ± SD; ***$P < 0.001$; Student's t test.

(H-I) Violin plots of expression level of seven macrophage plasticity associated markers with and without IL-11 (25 ng/mL) exposure. Data are mean ± SD; ***$P < 0.001$; Student's t test.

(J) CD163 and CD86 correlation scatter plot of macrophage showing the four subtypes based on mean value of CD163 and CD86. $P < 0.001$. Bar graph of subtype proportion with and without IL-11 (25 ng/mL) exposure.

(K) Flow cytometry histogram of CD163, CD206, CD209, and CD86 expression in primary macrophages from four treatment groups, included no treatment, M-CSF treatment, M-CSF + IL-11 (25 ng/ml) treatment, and M-CSF + IL-11 (100 ng/ml) treatment.

(L) Violin plots of log10 base expression level of CD163, CD206, CD209 and CD86 in primary macrophages from four treatment groups**.** Data are mean ± SD; ***$P < 0.001$; one-way ANOVA followed by Duncan's multiple range tests.

Figure S5 (related to Figure 4)

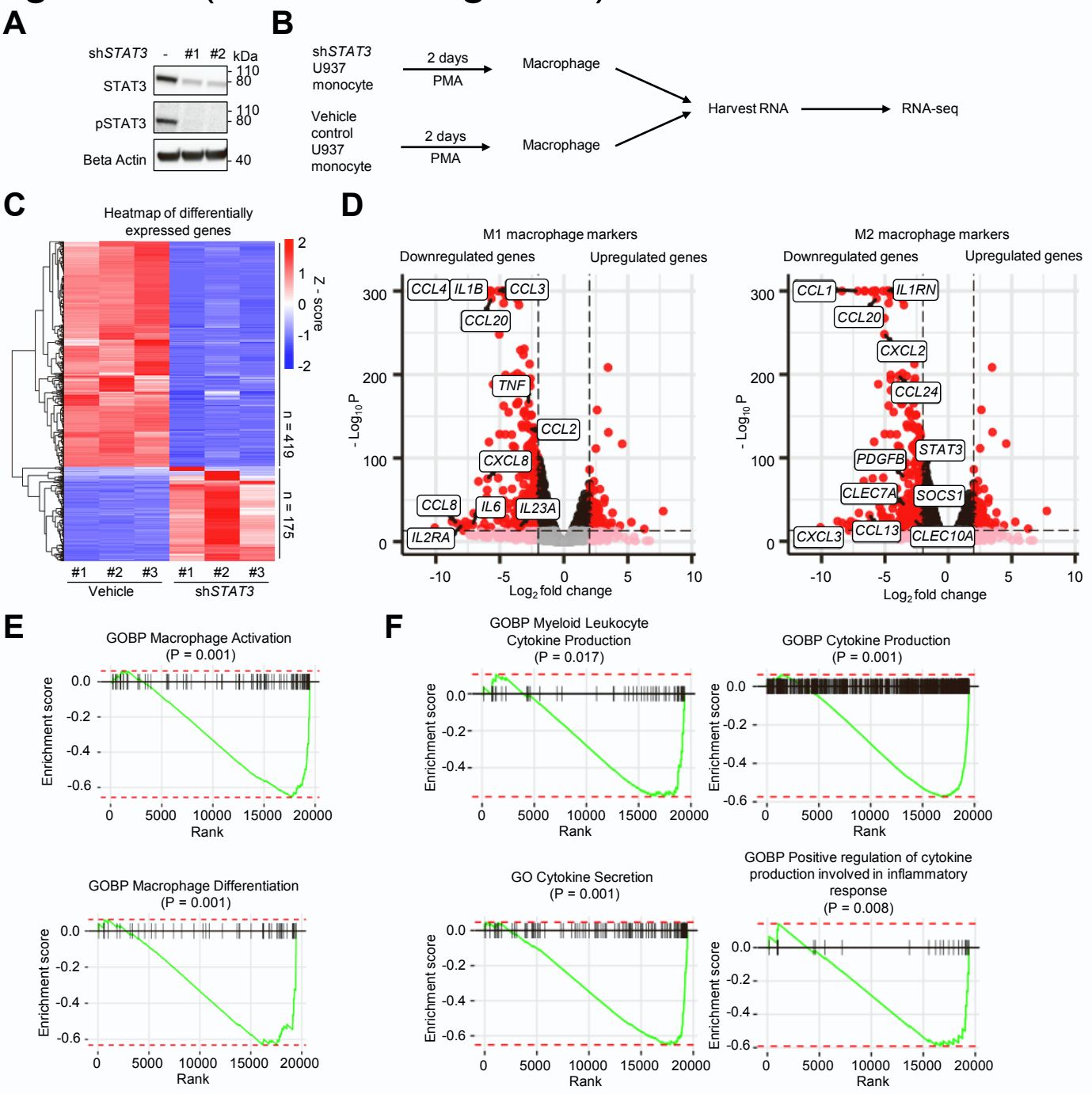

Figure S5. Macrophage function, differentiation, and cytokine expression were attenuated in *STAT3* knockdown U937-derived macrophages.

(A) Western blot analysis of STAT3 and phosphorylated STAT3 expression level in vehicle control and two clones of *STAT3* knockdown U937-derived macrophages.

(B) Flowchart of RNA-seq samples preparation.

(C) Heat map of differential expressed genes.

(D) Volcano plots illustrated down-regulation of M1 and M2 polarization markers.

(E-F) Gene set enrichment analysis (GSEA) reveal the attenuation of macrophage function, differentiation, and cytokine expression after *STAT3* knockdown.

Figure S6 (related to Figure 5)

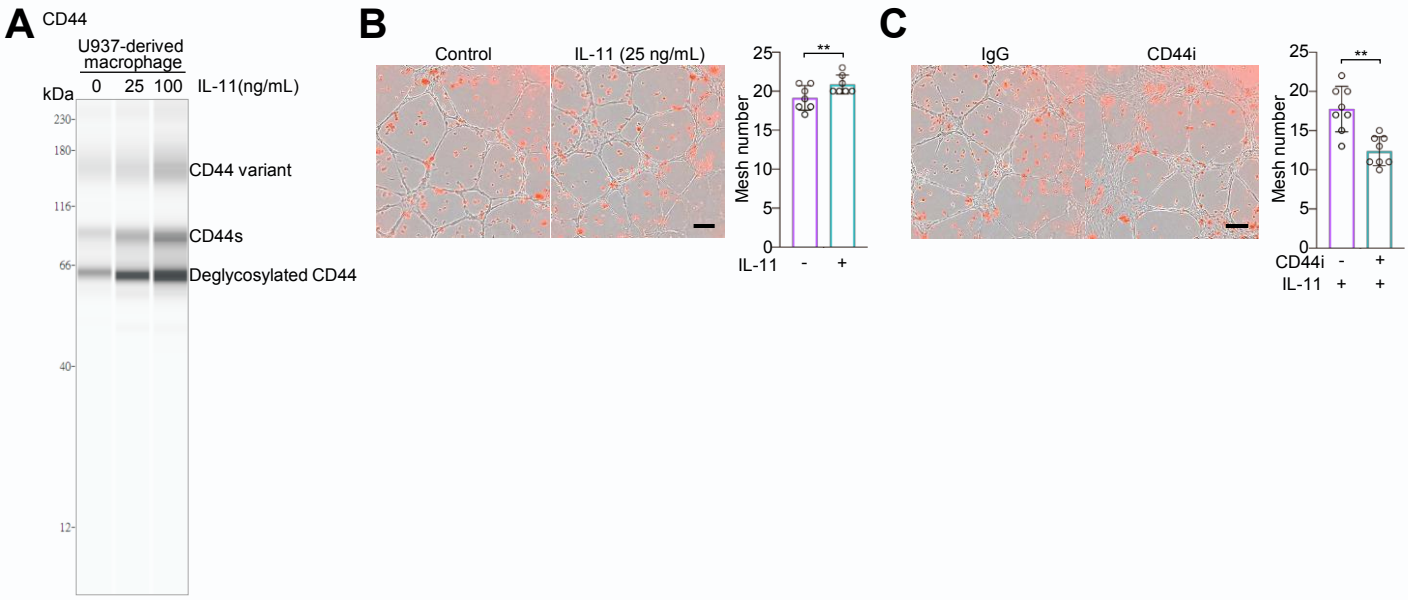

Figure S6. Second batch of vasculogenic assay to reveal AXL-IL-11-STAT3-mediated CD44 enhances vascular mimicry of macrophages (related to Fig. 5).

(A) Raw capillary Western immunoassay (WES) images of CD44 in U937-derived macrophages treated without or with IL-11 (25 ng/mL and 100 ng/mL).

(B) Bar graph of mesh number in HUVECs co-cultured with U937-derived macrophages pretreated with or without IL-11 (25 ng/ mL) (n=7). Data are mean ± SD; ** $P < 0.01$; Student's t test.

(C) Bar graph of mesh number in HUVECs co-cultured with U937-derived macrophages pretreated with IL-11 (25 ng/mL) and without or with CD44 inhibitor (n=8). Data are mean ± SD; ** $P < 0.01$; Student's t test.

Figure S7 (related to Figure 6)

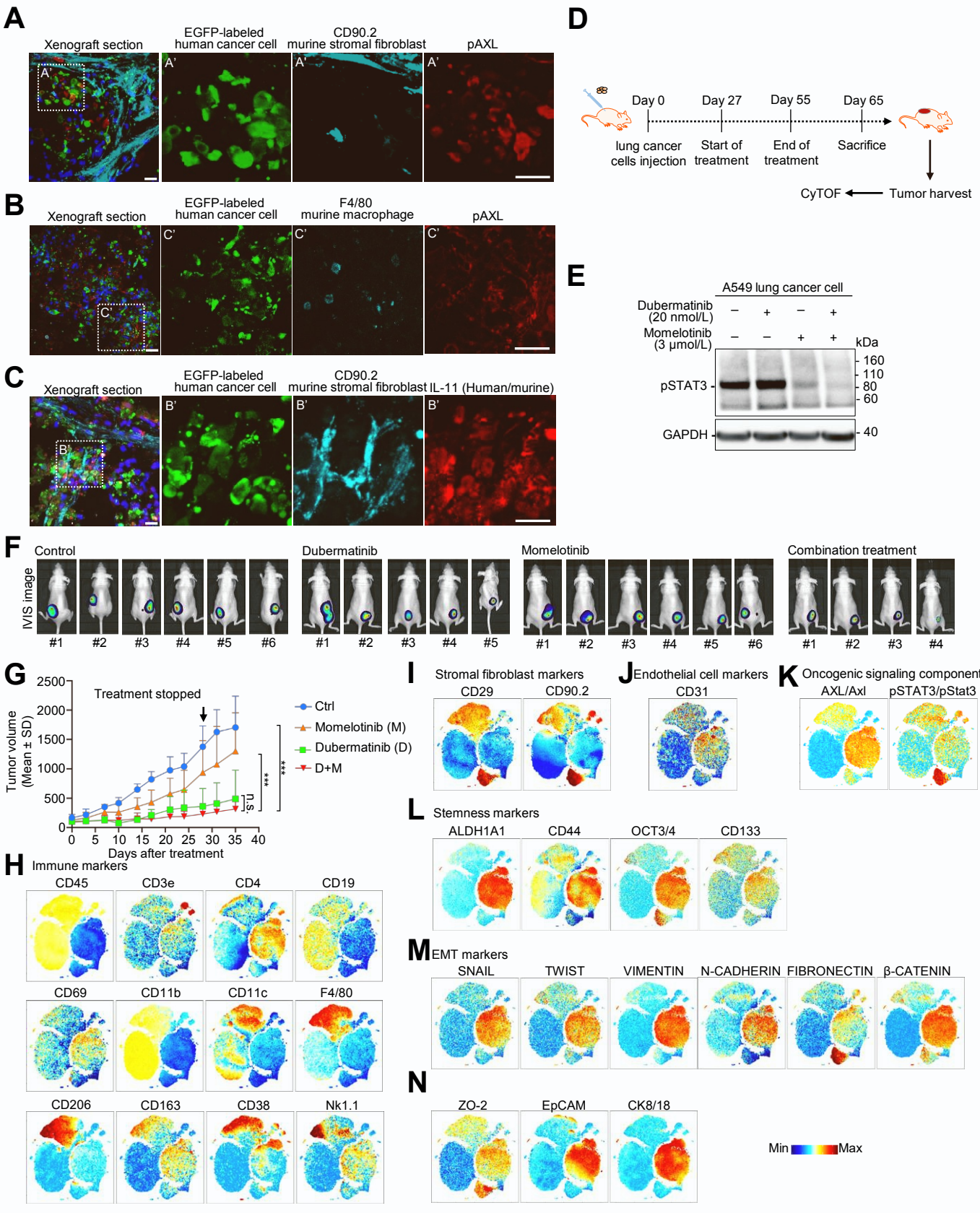

Figure S7. Combined targeting of AXL and STAT3 attenuated xenograft tumor growth (related to Fig. 6).

(A-C) Immunofluorescence images of xenograft tumor sections showing phosphorylated AXL and IL-11 expression among human cancer cells, murine macrophages, and murine stromal fibroblasts in the xenograft tumor microenvironment. Zoom-in images are shown in the right panels. Scale bar = 20 μm.

(D) Experimental workflow of mouse xenograft models.

(E) Western blots of phosphorylated STAT3 in A549 lung cancer cells treated with dubermatinib and/or momelotinib.

(F) Representative bioluminescent images of tumor bearing mice taken on Day 65 prior to sacrifice and tumor harvest.

(G) Growth curves of the average tumor size in 4 treatment groups: control (n=6); dubermatinib 90 mg/kg oral dose twice weekly (n=6) x 28 days; momelotinib 25 mg/kg oral dose once daily x 28 days (n=6); combined treatment x 28 days (n=6). Combined treatment reduced tumor volumes 80% compared with control (***$P < 0.001$). Dubermatinib dose decreased 20% to minimize toxicity. Data are mean ± SD; ***$P < 0.001$; one-way ANOVA followed by Duncan's multiple range tests.

(H-J) t-SNE scatter plots of expression levels of markers for murine immune cells, murine stromal fibroblasts, and murine endothelial cells.

(K-N) t-SNE scatter plots of expression levels of oncogenic signaling, stemness and EMT markers.

Figure S8 (related to Figure 6)

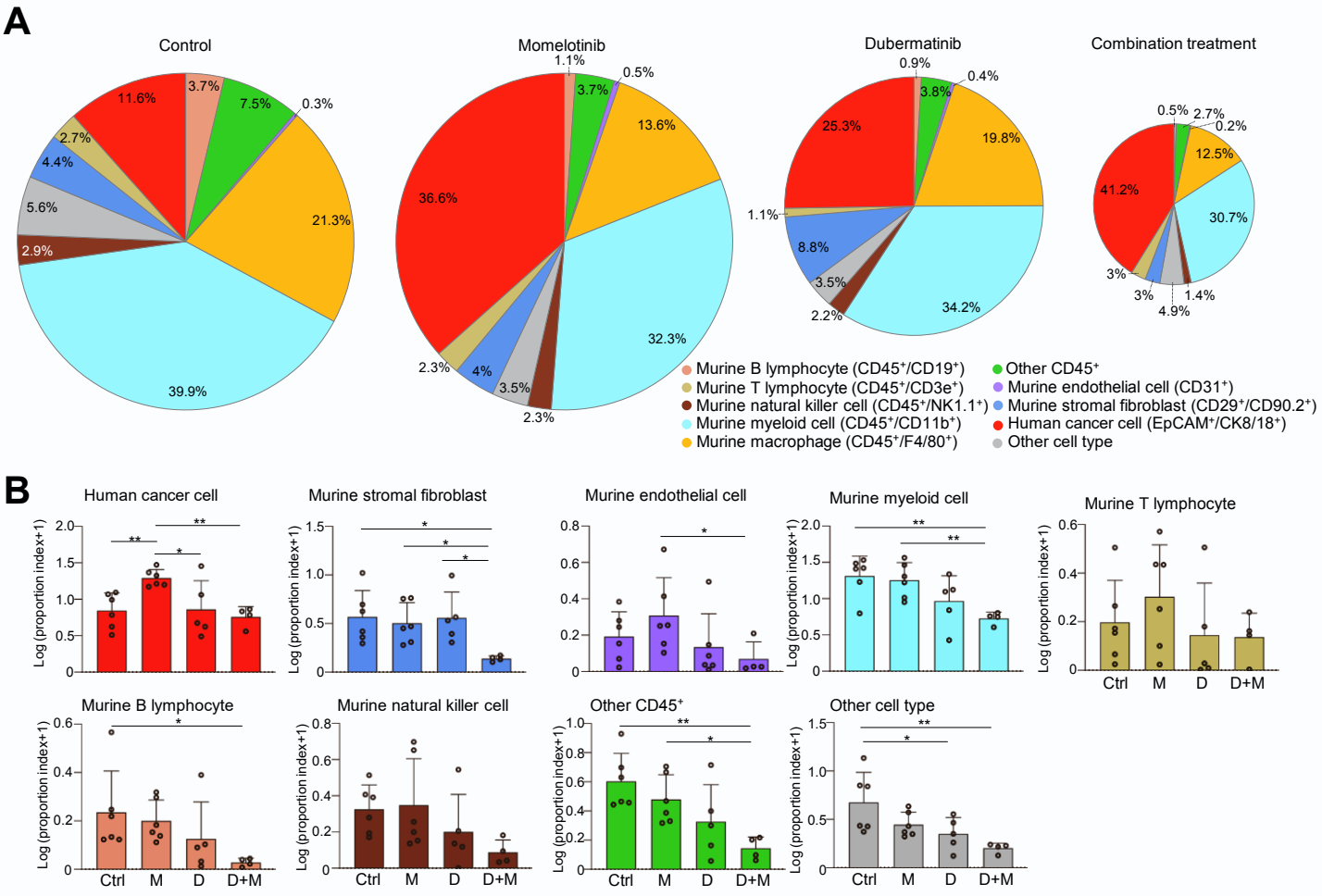

Figure S8. Combined targeting of AXL and STAT3 reconfigures cellular composition and disrupts host cell conscription in xenograft tumor microenvironments (related to Fig. 6).

(A) Pie charts of cell type proportion in the xenograft tumors of the four treatment groups.

(B) Bar graphs of nine cell type proportion index of the four treatments in log 10 base units (vehicle control (n=6), dubermatinib (n=5), momelotinib (n=6), and combination treatment (n=4)). Data are mean ± SD; *P < 0.05., **P < 0.01; one-way ANOVA followed by Duncan's multiple range tests.

Table S1. Clinicopathological information of lung cancer patients

Group	Patient ID	Age	Gender	Smoking status	Lung cancer type and specimen	Subtype	Differentiation	TNM classification	Stage	Max tumor size	EGFR	ALK	ROS1
2	Pt 002	80	F	Former smoker, quit 25 years ago	Adenocarcinoma (lymph node metastasis)			T1cN2M0	IIIA	3 cm			
2	Pt 004	74	F	Former smoker, 45 pack years	Invasive adenosquamous carcinoma (separate nodule)			T3N2M0	IIIB	2.1 cm			
2	Pt 006	54	F	Nonsmoker	Pleomorphic carcinoma with adenocarcinoma		Poor	T1cN1M0	IIB	2.1 cm	Exon 19 deletion	Negative	Negative
1	Pt 007	68	M	Current, 75 pack years	Adenocarcinoma	Acinar pattern		T2aN0M0	IB	3 cm	Negative	Negative	Negative
1	Pt 008	79	M	Current, 100 pack years	Invasive adenocarcinoma	Papillary and hepatoid		T2aN0M0	IB	3 cm			
2	Pt 009	82	F	Former smoker, 50 pack years	Invasive adenocarcinoma	Lepidic, solid and glandular	Moderate	T1cN2M0	IIIA	3.6 cm			Negative
1	Pt 010	57	F	Current, 45 pack years	Adenocarcinoma	Micropapillary, papillary and acinar	Moderate	T1bN0M0	IA	3.2cm			
1	Pt 012	82	F	Former smoker, 60 pack years	Invasive adenocarcinoma	Acinar predominant with micropapillary pattern and colloid features		T1aN0M0	IA	2.1 cm	Negative	Negative	Negative
1	Pt 014	75	F	Nonsmoker	Invasive adenocarcinoma	Acinar predominant		T1bN0M0	IA	2 cm	Exon 19 deletion		
1	Pt 016	73	M	Former smoker, 40 pack years	Invasive adenocarcinoma	Papillary predominant		T2aN0M0	IB	1 cm			
2	Pt 017	74	F	Nonsmoker	Invasive adenocarcinoma (pleural metastasis)		Well to moderate	T2bN0M1b	IV	4.1cm	Exon 19 deletion	Negative	Negative
1	Pt 018	72	F	Former smoker, 17 pack years	Invasive Adenocarcinoma			T1bN0M0	IA2	1.6 cm			
1	Pt 027	60	F	Smoked as teenager (40 years without smoking)	Invasive adenocarcinoma	Acinar predominant with a lepidic pattern also present	well to moderately differentiated	pT1bN0M0	IA2	1.2cm			
1	Pt 028	75	M	60 pack years	Invasive adenocarcinoma	Acinar predominant with papillary (40%)	well differentiated	T3N0M0	IIB	6.2 cm	Negative	Negative	Negative
1	Pt 029	60	M	Current, 44 pack years	invasive squamous cell carcinoma	Focal keratinization; separate tumor nodules of same histopathologic type (intrapulmonary metastasis in same lobe)		pT3N0M0	IIIA	1.6cm	Negative	Negative	Negative

Table S2. Antibody panel of cytometry by time-of-flight (CyTOF) for primary tumors and co-cultured cells

Metal tag	Antigen	Clone	Vendor	Cat. No.	Marker type
89Yb	CD45	H130	Fluidigm	3089003B	Immune marker
141Pr	CD3	UCHT1	Fluidigm	3141019B	Immune marker
142Nd	CD19	HIB19	Fluidigm	3142001B	Immune marker
145Nd	CD163	GHI/61	Fluidigm	3145010B	Immune marker
148Nd	CD16	3G8	Fluidigm	3148004B	Immune marker
175Lu	CD14	M5E2	Fluidigm	3175015B	Immune marker
176Yb	CD56	CMSSB	Fluidigm	3176003B	Immune marker
150Ne	CD86	IT2.2	Fluidigm	3150020B	Immune marker
162Dy	CD66b	80H3	Fluidigm	3162023B	Immune marker
149Sm	CD200	OX104	Fluidigm	3149007B	Stromal marker
159Tb	CD90	5E10	Fluidigm	3159007B	Stromal marker
170Er	STRO-1	STRO-1	R&D Systems	MAB1038	Stromal marker
163Dy	CD105	43A3	Fluidigm	3163005B	Endothelial marker
172Yb	PECAM	HEC7	ThermoFisher Scientific	MA3100	Endothelial marker
173Yb	EPCAM		R&D systems	AF960	EMT, epithelial marker
174Yb	Keratin 8/18	C51	Fluidigm	3174014A	EMT, epithelial marker
143Nd	N-Cadherin		R&D systems	AF6426	EMT
146Nd	ZO-2	3E8D9	ThermoFisher Scientific	374700	EMT
155Gd	Fibronectin	2F4	ThermoFisher Scientific	MA517075	EMT
156Gd	Vimentin		R&D systems	MAB2105	EMT
166Er	SNAI1		Sigma	SAB 2108482	EMT
167Er	TWIST1	927403	R&D systems	MAB6230	EMT
144Nd	ALDH1A1	703410	R&D Systems	MAB5869	Stemness
151Eu	CD133	170411	R&D Systems	MAB11331-100	Stemness
160Gd	OCT3/4	240408	R&D Systems	MAB1759	Stemness
169Tm	Nanog	N31355	Fluidigm	3169014A	Stemness
171Yb	CD44	IM7	Fluidigm	3171003B	Stemness
161Dy	AXL		R&D systems	AF154	Signaling
158Gd	pSTAT3	4/p-stat3	Fluidigm	3158005A	Signaling
165Ho	TGFBR2		R&D Systems	AF-241	Signaling
152Sm	SMAD2	31H15L4	ThermoFisher Scientific	700048	Signaling
164Dy	SMAD4	253343	R&D Systems	MAB2097	Signaling
165Ho	TGFBR2		R&D Systems	AF-241	Signaling
168Er	β-catenin	196624	R&D systems	MAB13292	Signaling

Table S3. Antibody panel of cytometry by time-of-flight (CyTOF) for xenograft tumors

Metal tag	Antigen	Clone	Vendor	Cat. No.	Marker type
148Nd	CD45	3G8	Fluidigm	3148004B	Immune marker
152Sm	CD3e		Fluidigm	3152004B	Immune marker
172Yb	CD4		Fluidigm	3172003B	Immune marker
142Nd	CD11c		Fluidigm	3142003B	Immune marker
145Nd	CD69	GHI/61	Fluidigm	3145010B	Immune marker
146Nd	F4/80		Fluidigm	3146008B	Immune marker
149Sm	CD11b	OX104	Fluidigm	3149007B	Immune marker
162Dy	CD163		abcam	ab182422	Immune marker
175Lu	CD38		Fluidigm	3175014B	Immune marker
169Tm	CD206		Fluidigm	3169021B	Immune marker
170Er	NK1.1		Fluidigm	3170002B	Immune marker
165Ho	CD31		Fluidigm	3165013B	Mouse endothelial marker
156Gd	CD90.2		Fluidigm	3156006B	Murine stromal marker
111Cd	CD29		Novus Biologicals	AF2405	Murine stromal marker
173Yb	EPCAM		R&D systems	AF960	EMT, epithelial marker
174Yb	Keratin 8/18	C51	Fluidigm	3174014A	EMT, epithelial marker
112Cd	ZO-2	3E8D9	ThermoFisher Scientific	374700	EMT
141Pr	VIMENTIN		R&D systems	MAB2105	EMT
143Nd	N-Cadherin		R&D systems	AF6426	EMT
155Gd	Fibronectin	2F4	ThermoFisher Scientific	MA517075	EMT
166Er	SNAI1		Sigma	SAB 2108482	EMT
167Er	TWIST1	927403	R&D systems	MAB6230	EMT
144Nd	ALDH1A1	703410	R&D Systems	MAB5869	Stemness
151Eu	CD133	170411	R&D Systems	MAB11331-100	Stemness
160Gd	OCT3/4	240408	R&D Systems	MAB1759	Stemness
171Yb	CD44	IM7	Fluidigm	3171003B	Stemness
153Eu	JAK1	413104	R&D Systems	MAB4260	Signaling
158Gd	pSTAT3	4/p-stat3	Fluidigm	3158005A	Signaling
161Dy	AXL		R&D systems	AF154	Signaling
168Er	β-catenin	196624	R&D systems	MAB13292	Signaling

Table S4. Clustering parameters of PhenoGraph clustering algorithm

Figure	Clustering parameters
Figure 1B	CD45, CD3, CD19, CD163, CD16, CD200, CD86, CD90, CD66b, CD105, STRO-1, PECAM, EpCAM, CK8/18, CD14, CD56
Figure 6C	CD29, CD11c, CD69, F4-80, CD45, CD11b, CD19, CD3e, TER-119, CD90.2, CD163, CD31, CD206, NK1.1, CD4, EpCAM, CK8/18, CD38

Table S5. Primer sequences of Chromatin Immunoprecipitation (ChIP)-qPCR

Gene	Sequences 5'	Sequences 3'
CD44	ACAACTAAGAAGCAGCCATAAT	AGTAAGTCATCCACAGGCA

Table S6. Primer sequences of Reverse Transcription (RT)-qPCR

Gene	Sequences 5'	Sequences 3'
CD44	CTTTGTGGCATTTATTCATCAGT	CCATTTAACAGGAGCCGT